Published in final edited form as:
Nat Mater. 2015 January ; 14(1): 66–72. doi:10.1038/nmat4125.

Chiral Templating of Self-Assembling Nanostructures by Circularly Polarized Light

Jihyeon Yeom[1], **Bongjun Yeom**[2], **Henry Chan**[3], **Kyle W. Smith**[4], **Sergio Dominguez-Medina**[4], **Joong Hwan Bahng**[5], **Gongpu Zhao**[6], **Wei-Shun Chang**[4], **Sung Jin Chang**[7], **Andrey Chuvilin**[8,9], **Dzmitry Melnikau**[8,10], **Andrey L. Rogach**[11], **Peijun Zhang**[6], **Stephan Link**[4], **Petr Král**[3,12], and **Nicholas A. Kotov**[1,2,5,*]

[1]Department of Macromolecular Science and Engineering, University of Michigan, Ann Arbor, MI 48109, USA

[2]Department of Chemical Engineering, University of Michigan, Ann Arbor, MI 48109, USA

[3]Department of Chemistry, University of Illinois at Chicago, Chicago, IL 60607, USA

[4]Department of Chemistry, Rice University, Houston TX 77005, USA

[5]Department of Biomedical Engineering, University of Michigan, Ann Arbor, MI 48109, USA

[6]University of Pittsburgh School of Medicine, Pittsburgh, PA 15260, USA

[7]Division of Material Sciences, Korea Basic Science Institute, Daejeon, 305-333, Republic of Korea

[8]CIC NanoGUNE Consolider, Tolosa Hiribidea 76, Donostia-San Sebastian, 20018, Spain

[9]Ikerbasque, Basque Foundation for Science, Alameda Urquijo 36-5, 48011, Bilbao, Spain

[10]Centro de Física de Materiales (MPC, CSIC-UPV/EHU), Po Manuel de Lardizabal 5, Donostia-San Sebastian, 20018, Spain

[11]Department of Physics and Materials Science and Centre for Functional Photonics (CFP); City University of Hong Kong, 83 Tat Chee Avenue, Kowloon, Hong Kong S. A.R.

[12]Department of Physics, University of Illinois at Chicago, Chicago, IL 60607, USA

Abstract

Chemical reactions affected by spin angular momenta of circularly polarized photons are rare and display low enantiomeric excess. High optical and chemical activity of nanoparticles (NPs) should facilitate the transfer of spin angular momenta of photons to nanoscale materials but such processes are unknown. Here we demonstrate that circularly polarized light (CPL) strongly affects self-assembly of racemic CdTe NPs. Illumination of NP dispersions with right- and left-handed CPL induces the formation of right- and left-handed twisted nanoribbons, respectively. Enantiomeric excess of such reactions exceeds 30% which is ~10 times higher than other CPL-induced reactions. Illumination with linearly polarized light and assembly in the dark led to straight nanoribbons. The mechanism of “templation” of NP assemblies by CPL is associated with

*To whom correspondence should be addressed. kotov@umich.edu (N.A.K.).

selective photoactivation of chiral NPs and clusters followed by their photooxidation. Chiral anisotropy of interactions translates into chirality of the assembled ribbons. The ability of NPs to retain polarization information, or the “imprint” of incident photons opens new pathways for the synthesis of chiral photonic materials and allows for better understanding of the origins of biomolecular homochirality.

Keywords

chirality; self-assembly; circularly polarized light; nanoribbon; chiroptical properties

Materials with nanoscale chirality are known to strongly rotate the polarization of linearly polarized (LinP) and circularly polarized light (CPL). Such optical effects in nanomaterials with different chiral geometries are being actively investigated as a part of chiral photonics and plasmonics.[1–8] The opposite effects, i.e. the transfer of spin angular momenta of circularly polarized photons to matter and its subsequent nanoscale or atomic restructuring, retaining the “memory” of circular polarization, are much less known. The possibility of such effects at atomic and nanometer scale is indicated by, for instance, the formation of spiral nano-needles with controlled helicity during laser ablation of bulk metallic tantalum with CPL,[9] although the mechanism of this effect is not well understood. The transfer of spin angular momenta in high intensity focused laser beams was also observed for Bose–Einstein condensates,[10] ensembles of cold atoms,[11] and microscale colloids.[12] These special chromophores/scatterers acquired circular or spiral motion while being illuminated by high intensity CPL. However, their achiral symmetry, structural barriers for channeling the rotational energy into chemical bonds, and fast quenching of rotational motion by the media make it difficult to translate physical motion into the permanent structural changes of these atomic and particulate systems.

The transfer of spin angular momentum was observed for a wide range of sizes and molar masses (M) of particles – from $M \approx 10^2$ for ensembles of cold atoms [11] to $M \approx 5 \times 10^{12}$ for microscale colloids.[12] It should be possible to observe some CPL effects for nanoparticles (NPs) that are intermediate in mass and size between atom clusters and microparticles and are similar to Bose-Einstein condensates ($M \approx 10^7$).[10] NP dispersions stable at ambient conditions are more convenient to use than some of these chromophores/scatterers and can be more reactive than polymeric colloids[12] or bulk tantalum.[9] The larger physical size of the NPs should enhance the photochemical effects of light with different handedness compared to those observed for chiral organic molecules.[13,14] CPL-induced restructuring of NP systems can provide a new, powerful, and versatile tool for investigating the (nano)chemistry of chiral materials. Interest in the synthesis of chiral nanostructures has been fueled by the potential application of chiral nanostructures in biosensing, telecommunication, display technologies, diffraction-free patterning, and chiral catalysis.[2–7] Further motivation to study long-term structural changes caused by CPL in matter is evidenced by the ongoing discussion about the origin of homochirality in natural compounds. Natural amino acids and sugars exist predominantly as left-handed (LH) and right-handed (RH) enantiomers, respectively. Illumination with CPL[15–17] was recently suggested as one of the plausible causes of homochirality.[17,18] However, the mechanism of

how CPL can lead to homochirality of organic molecules is not known. Several chemical routes are being debated,[15,16] including chiral amplification.[19,20]

Self-assembly of NPs is one of the mechanisms that could potentially be influenced by CPL. Such expectations are based on (a) atomic and nanoscale chirality of individual NPs,[21,22] (b) amplification of circular polarization effects in NP assemblies,[23,24] and (c) sensitivity of self-assembly processes to small changes in interparticle interactions.[25] Also, inorganic NPs represent a convenient building block for nanoscale synthesis, affording a variety of pathways to geometrically complex nanostructures.

Based on this hypothesis, we investigated the effects of CPL on the assembly of water-soluble NPs under ambient conditions. A dispersion of CdTe NPs, stabilized by achiral capping agent thioglycolic acid (TGA), was illuminated either by left- (LCP) or right-handed circularly polarized light (RCP) with a wavelength of 543 nm. Note that this CdTe dispersion revealed no circular dichroism (CD) peaks in the visible range (Fig. S1) and therefore has equal cumulative absorbance for LCP and RCP photons at 543 nm. From a previous study[26] we expected the formation of twisted nanoribbons but it was unclear whether polarization of light would have an effect on their assembly pattern and geometry. CPL-induced transformations of NPs were examined after 1, 12, 28, 35 and 50 h of illumination (Fig. 1A and 1B). The temporal progression of the products included short 50–200 nm rods (1 h) that evolved into 1–2 μm twisted nanoribbons (12 h) and subsequently into 2–3 μm longer nanoribbons (28 h). After 50 h of illumination, twisted nanoribbons with total lengths, pitch lengths, and diameters of 3 ± 0.5 μm, 800 ± 20 nm, and 50 ± 5 nm, respectively, were the predominant products of the photo-induced reaction (Fig. 1C, see SI). When nanoribbons were exposed to CPL for more than 90 h, they started to become thinner, but did not lose their acquired twisted shape (Fig. S2). In the absence of further illumination, the nanoribbons obtained after 50 h of photoinduced assembly retained their geometry for the entire project time (3.5 years).

Circular polarization of light exhibited a distinct photochemical influence on NP dispersions and the resulting geometry of twisted nanoribbon. Under LCP illumination, the majority of the products were left-handed (LH) nanoribbons as established by SEM (Fig. 1A and S3). When we illuminated the NP dispersion with RCP, right-handed (RH) nanoribbons of otherwise similar dimensions prevailed (Fig. 1B and S4). In both cases, the differences between LH and RH nanoribbon fractions obtained after analysis of 100 scanning electron microscopy (SEM) images of ~ 1000 nanoribbons were more than 30% (Fig. 1E), which was well in excess of the experimental error of ~5 %. Note that this is also much higher than a typical enantiomeric excess in CPL-stimulated organic reactions (0.5–2%).[14] The chiral preference in nanoribbon geometry was also confirmed by circular dichroism (CD) spectroscopy. CD spectra of purified nanoribbons were measured in aqueous dispersions and revealed distinct chiroptical bands at 490, 590, and 700 nm (Fig. 1F). Comparison of the spectral positions of the bands with the absorption spectra of similar dispersions after 50 h illumination (Fig. S6) indicates that the first two bands are associated with the absorption in the band-gap transition. Importantly, nanoribbon dispersions illuminated by LCP and RCP showed positive and negative CD signals, respectively. Transmission electron microscopy

(TEM) tomography (Fig. 2A, and B), capable of visualizing 3D structures of the nanoribbons, corroborated the conclusions regarding their chiral shape.

A control experiment involving illumination with un-polarized light (UnP) showed equal distribution between right- and left-handed nanoribbons in agreement with the previous study.[26] Illumination with LinP as well as incubation in the dark yielded straight nanowires that were the overwhelmingly dominant products in these two cases. Nanowires produced by exposure to UnP and LinP revealed no CD activity (Fig. S7) consistent with the SEM data (Fig. S9).

Another experimental series contributing to understanding of templating effect of photons on the mesoscale geometry of nanoribbons and nanowires was the illumination of CdTe dispersions with a different light source at 607 nm for 50 h. The efficiency of chiral induction by LCP is reduced as the difference between the yield of LH and RH nanoribbons drops to ~20% (Fig. S10) compared to illumination at 543 nm. This observation is consistent with the reduced intensity of NP absorbance at the fringes of the band gap transition (Fig. S1B).

In order to avoid the effects of chirality arising from potential artifacts of small molecular weight compounds present in solution, we compared CD spectroscopy of ensembles of chiral structures in dispersion with CD measurements taken for single nanoribbons (Fig. 2E and 2F) for the 600–800 nm spectral window. The single LH and RH nanoribbons revealed correspondingly positive and negative mirror-image CD signals. A band located at ~660–700 nm is spectrally similar to the band observed for dispersions (Fig. 1F; due to the technical limitations of single particle CD spectroscopy setups related to the calibration procedure of the quarter wave plates we presently cannot extend these measurements to the 600-400 nm region). Figs. S11 and S12 demonstrate that the CD spectra of the single twisted nanoribbons measured using dark field microscopy are dominated by scattering. The ‘red’ CD bands in Fig. 1F, therefore, should be attributed predominantly to scattering of LCP and RCP photons on twisted nanoribbons with specific handedness. As a control experiment against potential artifacts we measured CD spectra from single nanoribbons at various rotational angles in respect to the long axis. The shape of CD spectra remained unchanged regardless of incident angle (Fig. S13). As another control experiment, confirming attribution of the origin of the CD bands, non-twisted nanowire did not show any CD signals (Fig. S14).

The chiroptical properties of the twisted nanoribbons can be compared to those of microscale gold helixes made by 3D lithography[8] which also exhibit broadband polarization rotation. Anisotropy factors of g = 0.02–0.04 were obtained from numerical FEM solutions of the Maxwell equations for CdTe twisted ribbons models (Fig. 2C, and 2D), which is comparable to the values obtained for super Ag enhanced Au nanohelices and Au nanorods/fiber composites, $g \sim 0.025$.[2,3]

To understand how circular polarization of photons causes distinct permanent differences in shapes of nanoribbons, we first addressed the mechanism of light-induced self-assembly of CdTe NPs. From the optical properties (Fig. S7) and the relative content of NPs in the

supernatant of nanoribbons dispersions assembled with and without light (Fig. S15), it becomes apparent that, along with the spontaneous self-assembly of NPs,[26, 27] there is a parallel light-stimulated process of the formation of twisted ribbons. We found that FTIR peaks for ν(O-H), δ(O-H), ν_s(COOH), characteristic of TGA ligand located at 3500 cm^{-1}, 1567 cm^{-1}, and 1421 cm^{-1}, respectively, were drastically decreased in nanoribbons compared to the original CdTe NPs (Fig. 3A). A strong peak at 1722 cm^{-1} corresponding to ν_{as}(COO-) of carboxyl moieties was observed in the supernatant obtained after separation of twisted nanoribbons and NPs by centrifugation. Concomitantly, the characteristic UV-Vis absorption peak of TGA at 276 nm decreased as illumination time increased (Fig. S16), indicating its decomposition. The presence of an S 2p signal from CdS in X-ray photoelectron spectra (XPS) of nanoribbons (Fig. S17) and the weakness of peaks for Te from CdTe (Fig. S18) indicate that illumination also results in the replacement of Te in the NPs with S; the elemental atomic composition of nanoribbons were 51.5 % Cd, 47.3 % S, 1.2% Te (Table S1). The mechanism of photoinduced replacement of Te by S in NPs is likely to involve ionic diffusion of S^{-2} ions formed by photoinduced oxidation of TGA into the NPs. TEM of the twisted region (Fig. S19, and S20), atomic mapping images (Fig. S22), and energy dispersive spectroscopy (EDS) spectra (Figs. S23 and S24) confirmed the transformation of CdTe NPs into CdS NPs (Fig. 3B). These results are consistent with previous findings regarding formation of a thin CdS shell around CdTe NPs due to chemical decomposition of TGA (Supplementary Information) and photoinduced oxidation of CdTe.[28]

X-ray photoelectron spectroscopy spectra (Fig. S26) indicated that there was no significant difference in chemical composition of left and right-handed nanoribbons and, therefore, the assembly mechanism should be the same for RCP and LCP illumination. Spectroscopy and microscopy data in Fig. 3 and Figs. S16–S27 (see SI for details) suggest that the light-induced mechanism of nanoribbon self-assembly starts with the photoinduced decomposition of TGA to form S^{-2} that subsequently replaces Te^{-2} ions in NPs. The loss of the already sparse TGA shell is likely to be the trigger of the light-induced NP assembly into twisted structures. Such attribution of the self-assembly mechanism encounters, however, an unexpected complication. The electrokinetic zeta-potential, ζ, decreased from ~ −6 mV to ~ −15 mV upon illumination (Fig. S29); the increase in electrostatic repulsion must hinder the assembly process contrary to the results observed. Calculations of the pair-potentials between the NPs using extended Derjaguin-Landau-Verwey-Overbeek theory (E-DLVO) help to explain this discrepancy and confirm the light-induced assembly mechanism. Even though the zeta-potential of “bare” CdS NPs are more negative, the loss of the TGA shell and increased ionic strength associated with the surface ligand photooxidation makes the overall pair potential more attractive (Fig. S30).

Based on the above results, the effect of circular polarization of incident light on NP self-assembly originates in the optically selective activation of nanostructures with different handedness. Both individual CdTe NPs and their clusters can be chiral. As such, aberration corrected TEM tomography indicates the existence of chiral dislocations of atoms in Pt NPs.[22] Chirality of individual Au NPs in racemic mixtures capped with achiral ligands similar to TGA was previously shown with liquid chiral chromatography.[29] In respect to our

TGA-stabilized NPs, we observed that they have a shape of truncated tetrahedrons by high-angle annular dark field (HAADF) scanning transmission electron microscope (STEM) (Figs. 3G and 3H). The distinct truncated tetrahedron shape of CdTe-TGA NPs was also seen by high resolution TEM images as well (Fig. 3I). Four uneven truncations result in a chiral tetrahedron similar to a sp^3 hybridized carbon atom with three different substituents (Fig. S31). To confirm chirality of individual NPs, we incubated the dispersion of TGA-stabilized CdTe NPs with bovine serum albumin (BSA, 66.5 kDa) serving here as a enantioselective selective adsorber. After 5 hour incubation, we separated BSA and unbound NPs using centrifugal membrane (50 kDa), and measured CD spectra of obtained dispersions. In contrast to the original CdTe NPs that has no CD signals (Fig. S1) and BSA that has a negative CD peak at 215 nm (Fig. S34), the separated NPs showed positive CD band at 400–550 nm (Fig. S35) coinciding with the excitonic transition of NPs. This observation indicates that the starting NP dispersion is a racemic mixture of NP enantiomers with different chirality that can be enantioselectively separated.

Simulation of light absorption showed that enantiomers of truncated NPs (Fig. 3C, S31) display optical activity reflected in the mirror-imaged simulated CD and *g*-factor spectra (Fig. 3D). Spontaneously formed small clusters of NPs can also be chiral. According to our simulations, the differences in absorption of LCP and RCP in such clusters (Fig. 3F) are even greater than in NPs (Fig. 3D). In both cases, there is a large difference in absorption of LCP and RCP at 543 nm for nanostructures of different handedness used for this study. The chiral nomenclature for NPs and clusters depend on the positive (*L*) and negative (*R*) CD signals.

The mechanism of the chirality transfer from CPL to NP assemblies can then be described as follows. The original CdTe NP solution is racemic and contains equal amounts of left- and right-handed particles and small clusters. When a racemic mixture of CdTe NPs (Fig. S1A) is illuminated by LCP at 543 nm, a subpopulation of LH NPs and clusters absorb light more effectively (Fig. S36 step **2**) than RH NPs and clusters. The same is true for RH NPs/clusters (Fig. S36, step **2′**) when the dispersion is illuminated with RCP. The light-activated CdTe NPs undergo photooxidation of TGA stabilizers that transforms them into “bare” CdS NPs. Photooxidation of multiple TGA ligands on the surface of NPs requires multiple photons and, therefore, the difference in the probability of absorption of *L*- and *R*-photons multiplies over time. This process “locks in” and amplifies the differences between the NPs of opposite chirality in the initially racemic mixture.

The ligand-free CdS NPs display a much stronger propensity to self-assemble than ligand-protected, non-light-activated CdTe NPs of opposite handedness (Fig. S30). Because the self-assembly of NPs is very sensitive to the anisotropy of NP interactions,[27] the chirality of the constituent building blocks is reflected in the helicity of the resulting assemblies similar to the self-assembly of organic and biological macromolecules.

Atomistic molecular dynamics (MD) simulations were performed to clarify the origin of the observed ribbon helicity (see SI for details). Individual NPs were modeled as slightly smaller 3.6 nm tetrahedrons with a cubic CdS crystal lattice and a lattice constant of a = 0.582 nm (Fig. 4A). The tetrahedrons were asymmetrically truncated by the removal of 2, 3,

and 4 atom layers from three of the NP vertices to acquire a left or right chirality. The NPs surfaces were not coated with stabilizers, in accordance with the experimental results presented in Fig. 3 and Figs. S16–S27, indicating ligands removal in the process of photoactivation. However, the large CdS lattice polarity was reduced at the NP surfaces to one half of the vacuum value to account for potential residual ligands. NPs at different (homogeneous) charging states were simulated in accordance with experimental observations. The MD simulations were carried out with explicit water molecules and Cl^- counterions of the charged NPs (Fig 4A, SI) to precisely describe the solvent environment of the NP self-assembly process.

Initially, NPs of the same (*L* or *R*) handedness (Fig. 4B) were preassembled into a planar piece of nanoribbon (Fig. 4C) with packing similar to that observed before,[26] assuming that NPs of predominantly one handedness were prepared by photoexcitation with a circularly polarized light and self-assembled. Upon equilibration of the NP assemblies in an isothermal–isobaric ensemble at T = 300 K for ~ 5–10 ns, the planar nanoribbons acquired distinct twists. Importantly, the twist was opposite for NPs with opposite handedness. The average twist angle observed in the simulation of the nanoribbons made from CdS NPs was − 2.4° and +4.6° for LH and RH NPs (Fig. 4D and 4E), respectively, which corresponds to a pitch length of ~600–800 nm similar to the experimental pitch length of nanoribbons observed in Figs. 1 and 2.

These observations confirm the significance of NP chirality in guiding the ribbon assembly and the realism of the photon-matter chirality transfer via geometry-specific photoactivation of NPs. The nanoribbon twists observed in the MD simulations clearly originate in the chirality (truncations) of the NPs, promoted via molecular-field-assisted NP-NP interactions into a cooperative phenomenon. As the light-transformed NPs are still largely solvated in water, their self-assembly into ribbons proceeds mostly via their bulk van der Waals coupling and partial hydrophobicity. However, water molecules form a soft “cushion” layer between the NPs within the ribbons, which allows the NPs to partially translate and reorient with respect to each other in accordance with the needs imposed by their chirality. The experimental structures are partially disordered (Fig. S20) due to fluctuations of the NP size that translates into some variability of the pitch and non-close packing of NP lattice in the ribbon.

Vivid experimental demonstration of subtle differences in interparticle interactions between a priori chiral NPs leading to nanostructures with different chirality can be obtained for NPs with a stabilizing ligand made from *D*- and *L*-cysteine (Fig. 4F, and 4G.) These originally chiral NPs were self-assembled in the dark and produced submicron helices with distinctly different twist directions depending on the chirality of the building blocks.

In conclusion, we have demonstrated that circular polarization of light can be “imprinted” on nanoscale structures by altering the chirality of NPs participating in the self-assembly process. Because light-sensitivity is common for NPs (see SI for details) this study offers new synthetic methods for chiral nanostructures using light as the primary parameter determining the asymmetry in the enatiomeric mixture of the products. Furthermore, geological records suggest that inorganic NPs were a part of the primordial Earth

conditions,[30] and therefore, selective photonic activation of seemingly achiral NPs might represent the missing link between cosmic CPL[15–17] and inorganic/organic materials with preferential chirality.

Supplementary Material

Refer to Web version on PubMed Central for supplementary material.

Acknowledgments

This material is based upon work partially supported by the Center for Solar and Thermal Energy Conversion, an Energy Frontier Research Center funded by the U.S. Department of Energy, Office of Science, Office of Basic Energy Sciences under award number #DE-SC0000957, and ARO MURI W911NF-12-1-0407 “Coherent Effects in Hybrid Nanostructures for Lineshape Engineering of Electromagnetic Media” (N.A.K. and S.L.). We acknowledge support from NSF under grant ECS-0601345; CBET 0933384; CBET 0932823; and CBET 1036672. Financial support from the Robert A. Welch Foundation (C-1664) is also acknowledged (S.L.). The support from NIH grant GM085043 (P.Y.) is gratefully acknowledged. P.K. work was supported by the NSF DMR grant No. 1309765 and ACS PRF grant No. 53062-ND6. The authors thank Ms. Ji-Young Kim for assistance with chiral NP assembly experiments.

References

1. Ren MX, Plum E, Xu JJ, Zheludev NI. Giant nonlinear optical activity in a plasmonic metamaterial. Nat Commun. 2012; 3:833. [PubMed: 22588295]
2. Kuzyk A, et al. DNA-based self-assembly of chiral plasmonic nanostructures with tailored optical response. Nature. 2012; 483:311–314. [PubMed: 22422265]
3. Guerrero-Martinez A, et al. Intense Optical Activity from Three-Dimensional Chiral Ordering of Plasmonic Nanoantennas. Angew Chem Int Edit. 2011; 50:5499–5503.
4. Liu S, et al. Synthesis of chiral TiO_2 nanofibre with electron transition-based optical activity. Nat Commun. 2012; 3:1215. [PubMed: 23169056]
5. Hentschel M, et al. Optical Properties of Chiral Three-Dimensional Plasmonic Oligomers at the Onset of Charge-Transfer Plasmons. ACS Nano. 2012; 6:10355–10365. [PubMed: 23078518]
6. Mark AG, Gibbs JG, Lee TC, Fischer P. Hybrid nanocolloids with programmed three-dimensional shape and material composition. Nat Mater. 2013; 12:802–807. [PubMed: 23793159]
7. Hendry E, et al. Ultrasensitive detection and characterization of biomolecules using superchiral fields. Nat Nanotechnol. 2010; 5:783–787. [PubMed: 21037572]
8. Gansel JK, et al. Gold Helix Photonic Metamaterial as Broadband Circular Polarizer. Science. 2009; 325:1513–1515. [PubMed: 19696310]
9. Toyoda K, Miyamoto K, Aoki N, Morita R, Omatsu T. Using Optical Vortex To Control the Chirality of Twisted Metal Nanostructures. Nano Lett. 2012; 12:3645–3649. [PubMed: 22690654]
10. Brachmann JFS, Bakr WS, Gillen J, Peng A, Greiner M. Inducing vortices in a Bose-Einstein condensate using holographically produced light beams. Opt Express. 2011; 19:12984–12991. [PubMed: 21747450]
11. Tabosa JWR, Petrov DV. Optical pumping of orbital angular momentum of light in cold cesium atoms. Phys Rev Lett. 1999; 83:4967–4970.
12. Padgett M, Bowman R. Tweezers with a twist. Nat Photonics. 2011; 5:343–348.
13. Tang YQ, Cohen AE. Enhanced Enantioselectivity in Excitation of Chiral Molecules by Superchiral Light. Science. 2011; 332:333–336. [PubMed: 21493854]
14. Feringa BL, van Delden RA. Absolute asymmetric synthesis: The origin, control, and amplification of chirality. Angew Chem Int Edit. 1999; 38:3419–3438.
15. Green MM, Selinger JV. Cosmic chirality. Science. 1998; 282:880–881. [PubMed: 9841434]
16. Bailey J, et al. Circular polarization in star-formation regions: Implications for biomolecular homochirality. Science. 1998; 281:672–674.

17. Lucas PW, et al. UV circular polarisation in star formation regions: The origin of homochirality? Origins Life Evol B. 2005; 35:29–60.
18. Cronin JR, Pizzarello S. Enantiomeric excesses in meteoritic amino acids. Science. 1997; 275:951–955. [PubMed: 9020072]
19. Prins LJ, Timmerman P, Reinhoudt DN. Amplification of chirality: The “sergeants and soldiers” principle applied to dynamic hydrogen-bonded assemblies. J Am Chem Soc. 2001; 123:10153–10163. [PubMed: 11603964]
20. Smulders MMJ, Schenning APHJ, Meijer EW. Insight into the mechanisms of cooperative self-assembly: The “Sergeants-and-Soldiers” principle of chiral and achiral C-3-Symmetrical discotic triamides. J Am Chem Soc. 2008; 130:4204–4204.
21. Gautier C, Burgi T. Chiral N-isobutyryl-cysteine protected gold nanoparticles: Preparation, size selection, and optical activity in the UV-vis and infrared. J Am Chem Soc. 2006; 128:11079–11087. [PubMed: 16925425]
22. Chen CC, et al. Three-dimensional imaging of dislocations in a nanoparticle at atomic resolution. Nature. 2013; 496:74. [PubMed: 23535594]
23. Govorov AO, Fan ZY, Hernandez P, Slocik JM, Naik RR. Theory of Circular Dichroism of Nanomaterials Comprising Chiral Molecules and Nanocrystals: Plasmon Enhancement, Dipole Interactions, and Dielectric Effects. Nano Lett. 2010; 10:1374–1382. [PubMed: 20184381]
24. Ben Moshe A, Szwarcman D, Markovich G. Size Dependence of Chiroptical Activity in Colloidal Quantum Dots. ACS Nano. 2011; 5:9034–9043. [PubMed: 21967095]
25. Talapin DV, et al. Quasicrystalline order in self-assembled binary nanoparticle superlattices. Nature. 2009; 461:964–967. [PubMed: 19829378]
26. Srivastava S, et al. Light-Controlled Self-Assembly of Semiconductor Nanoparticles into Twisted Ribbons. Science. 2010; 327:1355–1359. [PubMed: 20150443]
27. Tang ZY, Kotov NA, Giersig M. Spontaneous organization of single CdTe nanoparticles into luminescent nanowires. Science. 2002; 297:237–240. [PubMed: 12114622]
28. Gaponik N, et al. Thiol-capping of CdTe nanocrystals: An alternative to organometallic synthetic routes. J Phys Chem B. 2002; 106:7177–7185.
29. Dolamic I, Knoppe S, Dass A, Burgi T. First enantioseparation and circular dichroism spectra of Au_{38} clusters protected by achiral ligands. Nat Commun. 2012; 3:798. [PubMed: 22531183]
30. Hartland A, Lead JR, Slaveykova VI, O’Carroll D, Valsami-Jones E. The Environmental Significance of Natural Nanoparticles. Nature Education Knowledge. 2013; 4:7.

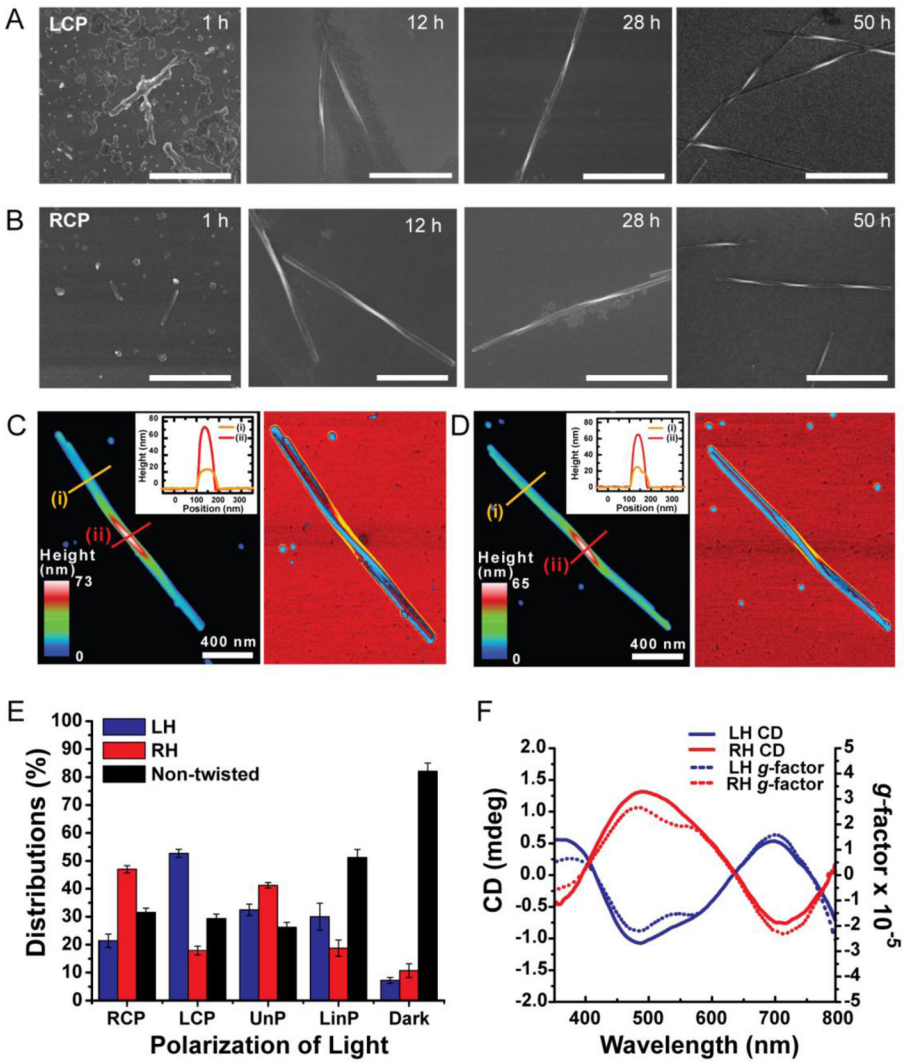

Figure 1. Self-assembly of CdTe NPs into twisted nanoribbons induced by illumination with CPL

A and **B,** SEM images of the ribbons assembled with LCP (A) and RCP (B) as a function of time exposure for 1 h, 12 h, 28 h and 50 h. All scale bars are 1 μm. **C** and **D,** tapping mode atomic force microscopy (AFM) topography (left) and phase (right) images of LH nanoribbon (C) and RH nanoribbon (D). **E,** Distributions of LH, RH, and non-twisted nanoribbons obtained after 50 h illumination with RCP, LCP, UnP, LinP light, and in the dark. **F,** ensemble CD spectra (solid line) and *g* factor (dotted line) of dispersions of left-handed (LH) nanoribbons and right-handed (RH) nanoribbons obtained after 50 h of CPL illumination. Linear dichroism effects that could be associated with adsorption on the walls of the cuvette and other spontaneous alignment of linear nanostructures have negligible contribution to the chiroptical properties as indicated by the identity of the CD spectra obtained with and without stirring of the dispersion.

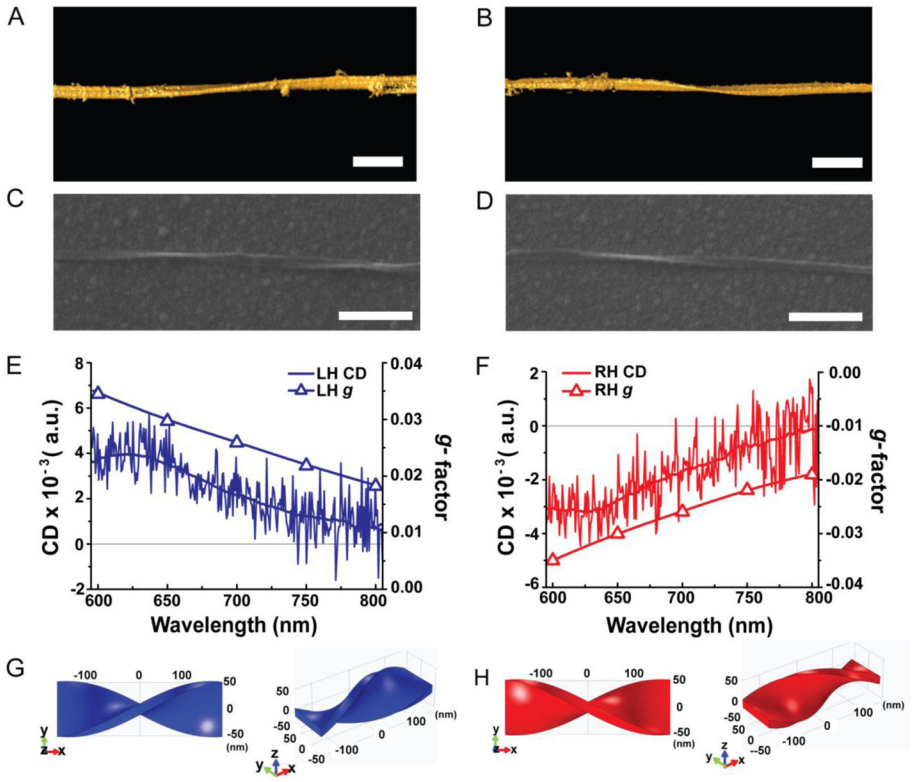

Figure 2. Chirality of single nanoribbons

A and **B,** Surface rendering of 3D TEM tomographic reconstruction of LH nanoribbon (A) and RH nanoribbon (B). Scale bars are 100 nm. **C** and **D,** SEM images of single LH (C) and RH nanoribbons (D). Scale bars are 500 nm. **E** and **F,** CD spectra and calculated *g*-factor spectra for single LH (E) and RH (F) nanoribbons in C and D, respectively. **G** and **H,** Computational models of the LH (G) and RH (H) nanoribbons used in the FEM calculations of chiroptical properties based on numerical solutions of Maxwell equations. All scales are nm.

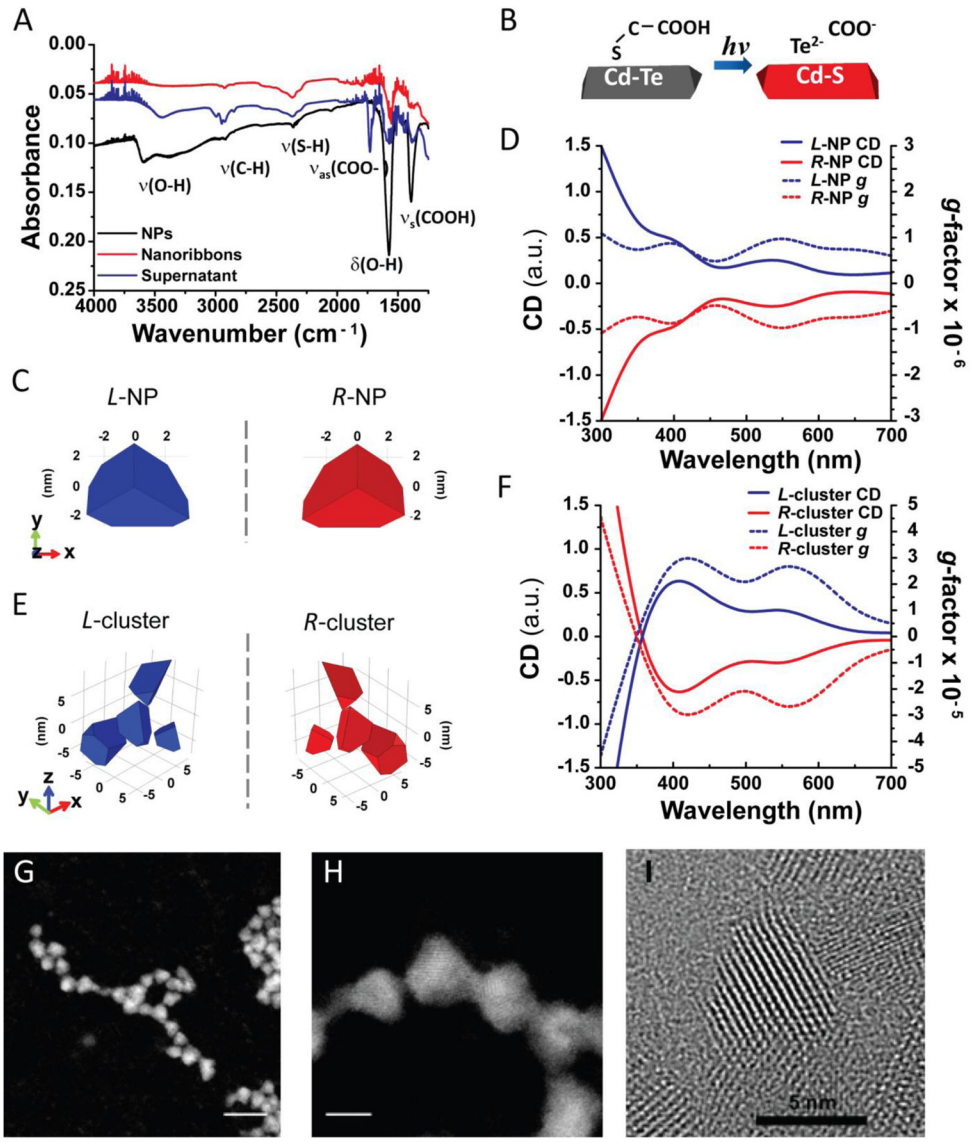

Figure 3. Mechanism of enantioselective assembly of NPs

A, FTIR spectra of original CdTe NPs, purified nanoribbons, and supernatant obtained after 50 h of illumination time. **B**, Schematic illustration of CdTe phase transition to CdS. **C,** and **E**, Models of chiral NPs (C) and chiral NP clusters (E) used in calculations of chiroptical properties. **D,** and **F,** Simulated spectra and *g*-factors for (D) *L*/*R*-NPs and (F) *L*/*R*-clusters of NPs. Nomenclature for NPs and their clusters is based on the positive (*L*) and negative (*R*) optical activity. **G,** and **H,** HAADF STEM images of TGA-stabilized truncated tetrahedral CdTe NPs. Scale bars are 15 nm (G) and 5 nm (H). **I,** High resolution TEM image of TGA-stabilized truncated tetrahedral CdTe NPs.

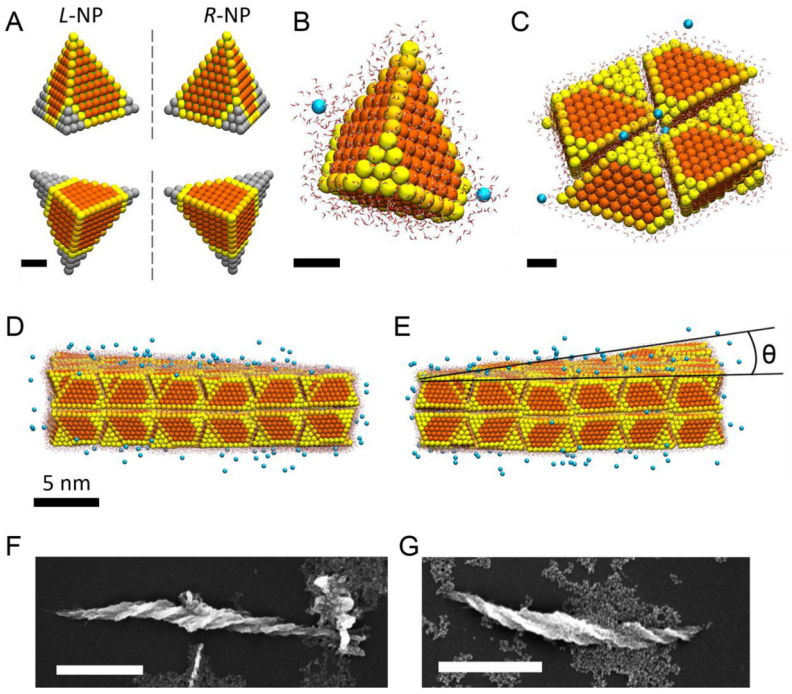

Figure 4. Molecular dynamic and experimental studies of self-assembly of chiral NPs

A, Atomistic models of NPs with LH and RH truncations used in MD simulations. **B,** Detailed view of a single NP in aqueous environment with counter ions used in MD simulations. **C,** A fragment of the simulated self-assembled ribbon from (top view) displaying packing of NPs. Scale bars in A, B, and C are 1 nm. **D,** and **E,** The side views of simulated NP ribbon with LH (D) and RH (E) truncated NPs. Dihedral angle θ determines the pitch of the nanoribbons. **F,** and **G,** SEM images of experimental assemblies spontaneously formed in dark from chiral CdTe NPs stabilized by L-cysteine (F) and D-cysteine (G). Scale bars are 1 μm.